Comparing methods of identifying non-stationary, non-linear processes from stream temperature time series data

Partington, D.[1], Shanafield, M.[2*] and Turnadge C.[3]

[1]College of Science and Engineering and National Centre for Groundwater Research and Training, Flinders University, Adelaide, Australia. (Daniel.Partington@flinders.edu.au; ORCID 0000-0003-2266-824X)

[2]College of Science and Engineering and National Centre for Groundwater Research and Training, Flinders University, Adelaide, Australia. (Margaret.Shanafield@flinders.edu.au; ORCID 0000-0003-1710-1548)

[3]CSIRO Land and Water, Adelaide, South Australia. (Chris.Turnadge@csiro.au; ORCID 0000-0002-9882-1573).

Corresponding author: Margaret Shanafield (Margaret.Shanafield@flinders.edu.au)

Key Points:

- Ephemeral streamflow events were successfully identified from stream temperature time series data using seven time series analysis methods
- Compared reductions in the amplitude of the diurnal temperature signal of stream water compared using seven time series analysis approaches
- For the specific case study assessed, the continuous wavelet transform was found to be the most efficacious and most parsimonious method

Abstract

The determination of flow state remains an important challenge in non-perennial river catchments. Previous studies interpreted stream channel temperature time series data using the moving standard deviation method to identify the timing and duration of flow. However, the performance of this technique requires the user to specify multiple subjective constraints. We implemented six variations of time-frequency analysis from three categories: (1) Fourier transform methods, (2) wavelet transform methods, and (3) Empirical Mode Decomposition methods. We evaluated and compared their ability to discern periods of flow from synthetic and field data of stream temperature time series data. Overall, all methods performed reasonably well, with performance of 63–99 % success in matching flow and no-flow periods. Greater variability in performance was observed when evaluating field data. Differences between methods include the ease of implementation and evaluation of results, computational needs, and ability to handle discontinuous data. We suggest five primary areas for future research to improve the general understanding of these time-frequency analysis techniques.

Plain Language Summary More than half of the world's rivers have no surface flow for some part of the year. In these rivers, measuring which parts of the catchment surface water network are flowing remains a key challenge to a full understanding of habitat connectivity, groundwater recharge, and other key ecosystem services. Temperature measurements have been used to identify flow state (i.e. periods of flow or no-flow) in rivers in previous studies, in which the moving standard deviation of time series data was typically calculated, and conditions applied to the results to identify periods of flow. In this study, we tested six variations of time-frequency transforms for identifying stream flows from temperature time series data. We found that all of these transforms worked well, with subtle differences in their performance, assumptions, and ease of use. The main advantage of these transforms over the moving standard deviation analysis is the avoidance of subjective criteria when determining flow states.

1. Introduction

Non-perennial river networks constitute over half of total river length worldwide (Datry et al., 2014). However, knowledge of the spatial and temporal variability of non-perennial flows is often limited (Costigan et al, 2017) and stream gauging networks are typically biased toward perennial rivers (De Girolamo et al., 2015; Eng et al., 2016). Even where gauges on non-

perennial rivers exist, often insufficient data are available to identify spatial variations in flows within a catchment. However, since the duration and volume of surface flows control both the availability and quality of water for flora and fauna along stream reaches (Datry et al., 2016), as well as the potential for groundwater recharge (Morin et al., 2009; Shanafield et al., 2012; Tooth, 2000), identifying and quantifying non-perennial flow patterns is critical.

The need for low-cost technologies that can be widely deployed has spurred several efforts to develop methods of streamflow detection and quantification beyond the traditional gauging station. The availability of inexpensive, easily programmable devices has led to the development of several types of streamflow monitoring devices, including electrical resistance sensors (Fritz and Johnson, 2006; Adams et al., 2006; Blasch et al., 2002; Goulsbra et al., 2009; Jaeger and Olden, 2011; Peirce and Lindsay, 2013; Jensen et al., 2019), float switch state loggers (Epting et al., 2018; Assendelft and van Meerveld, 2019), and temperature sensors (Blasch et al., 2004; Assendelft and van Meerveld, 2019). Combinations of sensors have been developed to provide more accurate determination of flow presence in certain settings, such as in headwater streams (Assendelft and van Meerveld, 2019) or where ice forms in a channel (Chapin et al., 2014). The use of temperature sensors on (or in) a streambed has received a great deal of attention, because temperature remains one of the easiest physical states to monitor. A variety of small, readily deployable, and relatively inexpensive loggers are now available. These loggers can often be secured to streambeds that sustain frequent scouring (Rodríguez-Burgueño et al., 2017), which is common in non-perennial rivers. Unlike flow meters, pressure transducers, or float sensors, they typically do not contain moving parts or openings that can become clogged with sediment. While a multitude of studies have used temperature time series pairs to calculate vertical flux rates in the shallow streambed of perennial streams (e.g. Rau et al., 2017), relatively fewer studies explored the use of paired temperature loggers to quantify vertical fluxes below non-perennial rivers. Even fewer studies used loggers on the streambed surface to identify surface flows.

In one of the earliest uses of temperature data to identify the presence or absence of streamflow, Constantz et al. (2001) used longitudinal changes in streambed temperature compared to a “benchmark” sensor (e.g. a sensor at stream gauge or other location where the presence of streamflow is known) to qualitatively evaluate the frequency and duration of downstream flows. The authors suggested installing sensors 0.15 m into the streambed to

minimize atmospheric noise, which had confounded their analysis. Used this approach of burying temperature sensors, Gungle (2005) detected periods of streamflow within a catchment by identifying a critical temperature drop that signaled the onset of streamflow. Rau et al. (2017) also examined longitudinal changes in temperature but concluded that temperature measurements alone were insufficient to detect streamflow. They further developed the amplitude ratio method commonly used to estimate vertical streambed fluxes (i.e. comparing temperatures measured at the surface and buried in the streambed) to also detect the presence of unsaturated conditions, in order to understand streamflow permanence.

Blasch et al. (2004) addressed the problem of "noise" measured by in-stream temperature devices by applying a moving standard deviation technique to the time series data. This method highlighted variations due to infiltration while removing long-term fluctuations. This technique was further improved by van Assendelft and van Meerveld (2019) who included additional criteria in their temperature measurement analyses. These were derived from visual inspection of temperature and flow data patterns from several monitoring stations in their study catchment. The authors found that periods of zero flow greater than three hours' duration could be identified from temperature time series, although precise estimation of timing of changes between flowing and no-flow conditions was not possible.

To date, quantitative temperature time series methods to identify the presence of surface flows have typically used conventional time series modeling methods, such as the Fourier transform (e.g. Rau et al., 2017). While such methods are well-established, their accuracy is limited by assumptions of linearity and stationarity (Jothiprakashet al., 2009). Here, we explore alternative analysis methods that avoid these assumptions. Several time-frequency (TF) transforms have evolved for the analysis of non-stationary time series data (Thakur et al., 2013; Dadu and Deka, 2016). TF transforms have previously been used within the hydrologic literature examining intermittent streamflow. Wavelets, for example, have been shown to be more useful than classical Fourier transforms for identifying long-term patterns of intermittency in rivers (Labat et al. 2005a,b). They have also been used within the pre-processing of flow and rainfall data to remove deterministic components in the data such as trends, variance, and daily or seasonal cycles before streamflow forecasting methods such as artificial neural networks were applied (Abdollahi et al., 2017; Maier and Dandy, 2000). To our knowledge, TF transforms have not been applied to streambed temperature time series data for flow state prediction.

In the present study we take advantage of time series data of stream stage, which indicates flow within the stream channel, and the temperature measured at the surface of the streambed. In a non-perennial river, this time series of temperature data would reflect local air temperatures during periods of no-flow and the temperature of the well-mixed stream discharge during periods of flow (Figure 1). Air and surface water temperatures both oscillate over seasonal and diurnal cycles (i.e. one cycle per year and one cycle per day, respectively). For investigations of flow presence, the diurnal cycle provides the most useful information.

A variety of methods is available to extract amplitude and phase information from temperature time series over a range of frequencies. These methods are continuously evolving, with various modifications offering advantages in certain applications. We selected six methods for comparison from three categories: (1) Fourier transform methods, including the short-time Fourier transform; (2) wavelet transform methods including the continuous wavelet transform (CWT) and synchrosqueezed CWT; and (3) empirical mode decomposition (EMD) methods, including the EMD with Hilbert-Huang transform, the Complete Ensemble Empirical Mode Decomposition with Adaptive Noise, and the Nonlinear Mode Decomposition. The theoretical basis of each method is briefly described in Section 2. The performance, advantages, and disadvantages of each method are described in Section 3. Additionally, the moving standard deviation (MSD) technique used in previous studies was computed for comparison. The basis for comparisons was defined in terms of the ability to identify flow presence. Three examples were used for comparison purposes: two synthetic cases featuring either low or high amplitude signal noise, and one field data example.

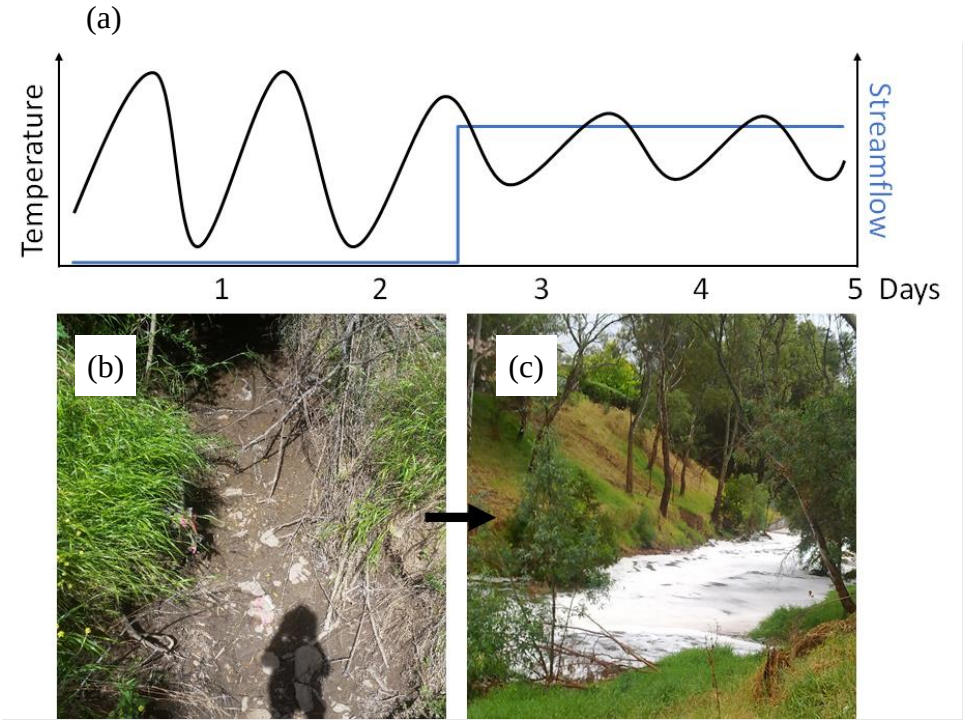

Figure 1. (a) Conceptual model of the relationship between the temperature recorded by a sensor installed on the streambed surface and the observed streamflow. When the stream is not flowing (b), the sensor records daily air temperature oscillations, but rapidly equilibrates with the temperature of the water during periods of flow (c).

2. Theory

Seven methods were compared: (1) short-time Fourier transform (STFT); (2) continuous wavelet transform (CWT); (3) synchrosqueezed CWT; (4) empirical mode decomposition with Hilbert-Huang transform; (5) complete ensemble empirical mode decomposition with adaptive noise (CEEMDAN); (6) nonlinear mode decomposition (NMD); and (7) moving standard deviation (MSD).

2.1. Short-time Fourier transform

The short-time Fourier transform (STFT; also known as the sliding window Fourier transform, or windowed Fourier transform) involves calculating the discrete Fourier transform (DFT) of a given time series over a given subset (i.e. window) size and advancing the window position by a uniform time increment through the duration of the original time series (Jacobsen and Lyons, 2003). In this manner, amplitude and phase results are calculated continuously through time, and are calculated over the windowed, rather than total, time series duration.

153 However, when applying the STFT, non-stationary processes that occur over timescales
154 that are smaller than the window size are difficult to detect. In addition, the resolution of DFT
155 results is inversely proportional to input dataset length. For this reason, a distinct trade-off occurs
156 between window size and the resolution required in Fourier transform results in order to
157 accurately quantify energies at specific frequencies. For example, larger window sizes will
158 enable greater separation between component frequencies, but the amplitude and phase values
159 calculated at these frequencies will be quantified over a larger timeframe. In particular, if abrupt
160 changes in frequency amplitudes and/or phases occur then these will be difficult to detect, due to
161 the "smearing" effect of the STFT.

162 The limitations of the STFT have been recognised for decades (e.g. Rudi et al., 2010).
163 For this reason, published applications of the STFT in hydrology and related fields are scarce.
164 Instead, following their development in the 1990s, wavelet transforms were incorporated into
165 STFT approaches. For example, Kunkel and Pierce (2009) combined wavelet basis functions and
166 the STFT approach to identify the timing of peak snowmelt events at 28 gauged sites in Idaho,
167 USA over a 12-month period. The efficacy of the method was assessed through comparisons to
168 measured snowmelt fluxes. Using the STFT, peak snowmelt dates were estimated to within ±4
169 days accuracy during approximately 95 % of the study period, and to within ±7 days accuracy
170 during the entire study period. In the present study, the STFT was provided as a basis for
171 comparisons with other methods, as it is conceptually the simplest of the time-frequency
172 methods and highlights the advantages of newer, alternative methods. The STFT was
173 implemented using the Python Numpy library (van der Walt et al. 2011). To minimize spectral
174 leakage, Hanning window filtering was applied prior to calculation of the discrete Fourier
175 transform.

176 **2.2. Continuous wavelet transform**

177 Wavelet transforms provide an alternative to Fourier transforms, which are based on
178 trigonometric basis functions. Unlike Fourier analysis, which uses a single sinusoidal basis
179 function type , a range of basis functions may be used in wavelet analyses. Unlike spectral
180 analyses, wavelet-based methods detect the distribution of periodic variabilities over a given
181 time span, rather than the average periodicities present (Andreo et al., 2006). Wavelet transforms
182 are widely used in a range of fields, including image analysis and compression, as well as a

variety of signal processing applications. The use of wavelet transforms was first introduced to Earth sciences by Grosmann and Morlet (1984); specifically, for the interpretation of seismic signals. Applications of wavelet transforms for time series analysis in hydrology were reviewed by Sang (2013) and Rhif (2019).

The theoretical development of wavelet transforms was described by Daubechies (1992) and Daubechies et al. (2000). Wavelet basis functions (w) are described as (Daubechies, 1990):

$$w(t,a,b) = \int_{-\infty}^{+\infty} \frac{1}{\sqrt{a}}\, \psi\left(\overline{\frac{t-b}{a}}\right) dt \qquad \text{Equation 1}$$

where a is a scaling parameter and b is a time shift parameter, for which values of 2 and 1 are commonly specified respectively (Daubechies, 1992; Sang, 2013). The continuous wavelet transform (CWT) is used to convolute a specified wavelet type (w) with a time series of interest $[x(t)]$; i.e. (Percival and Walden, 2006):

$$W(t,a,b) = \int_{-\infty}^{+\infty} x(t) \frac{1}{\sqrt{a}}\, \psi\left(\overline{\frac{t-b}{a}}\right) dt = \int_{-\infty}^{+\infty} x(t)\; w(t,a,b)\; dt \qquad \text{Equation 2}$$

Applications of the CWT to hydrological time series analysis include Labat et al. (2000a, 2000b), Andreo et al. (2006), and Niu and Sivakumar (2013). Labat et al. (2000a) used Fourier and convolution-based methods to quantify the correlation between karstic spring discharge and precipitation at study sites located in the Pyrenees Mountains, France. It was found that convolution models could not adequately simulate precipitation-discharge dynamics, and that Fourier methods were unable to characterize spring discharge rates. In particular, the methods were unable to characterize non-stationary processes and dynamics. In a companion paper (Labat et al., 2000b) the authors instead used both the continuous and discrete wavelet transform (DWT) to characterize both data types. Morlet and Haar wavelets were used for CWT and DWT analyses respectively. Time-dependent correlations were subsequently quantified via cross correlation analyses. Wavelet transforms enabled discrimination between rapid responses associated with horizontal karstic flow and slow responses associated with the vertical infiltration of recharge. Andreo et al. (2006) used the CWT to characterize karstic spring discharge, precipitation and air temperature time series data from the Iberian Peninsula, Spain. Annual periodicities of precipitation and temperature were found to remain constant over more

than 100 years. Shorter periodicities of 0.5, 2.5 and 5.0 years were also observed, which were consistent with observations from other areas of Europe. Niu and Sivakumar (2013) characterized daily streamflow data recorded near Wuzhou on the West River, a tributary of the Pearl River in southern China. Significant contributions to spring discharge from were identified at two timescales: 6–30 days (representing short-term processes) and one year (representing long-term processes). The latter were hypothesized to result from climatic drivers such as the Indian Ocean Dipole and the El Nino-Southern Oscillation. The authors applied the CWT to the entire dataset and did not use its unique properties to assess whether contributing processes were non-stationary. In the present study, the CWT featuring the Morlet wavelet type with parameters a=2 and b=1 was implemented using the Wavelet Toolbox for MATLAB (Misiti et al., 1996).

2.3. Synchrosqueezed CWT

The process of "synchrosqueezing" refers to improving the separation between dominant frequencies in a spectrum. This is achieved via a change in the basis used for the CWT, from parameters that specify scale and shift (i.e. a and b) to parameters that specify shift and instantaneous frequency (i.e. b and ω). The instantaneous frequency associated with any given pair of parameters (a, b) is calculated as (Daubechies et al., 2011):

$$\omega(a,b) = \frac{-i}{W}\frac{\partial W}{\partial b} \qquad \text{Equation 3}$$

The synchrosqueezed transform based on the instantaneous frequency ω is then given as the following indefinite integral with respect to the scale parameter, a:

$$T(\omega,b) = \int_{-\infty}^{+\infty} W(t,a,b)\ a^{-3/2}\ \delta[\omega(a,b)-\omega]\ da \qquad \text{Equation 4}$$

The theoretical development of the synchrosqueezed CWT (SCWT) was described by Daubechies and Maes (1996) and Daubechies et al. (2011). Use of the SCWT in Earth sciences has been limited, including applications in hydrology (Coleborn et al. 2013), paleoclimatology (Thakur et al., 2013), seismology (Hererra et al., 2014) and oceanography (Bian et al., 2018).

Coleborn et al. (2013) characterized water drip rates at 12 locations in Glory Hole Cave, a karst cave located in Yarrangobilly Caves National Park in southeastern Australia. Correlations between transformed drip rate data and SCWT-transformed barometric pressure, air temperature

and evapotranspiration data recorded at ground surface were used to identify casual mechanisms. Daily and sub-daily oscillations featuring variable temporal and spatial signatures were identified. The authors identified a single hypothesis that was consistent with all available data and hydrologic theory: that daily fluctuations in drip rate were driven by variations in tree water use. From this it was inferred that overlying tree roots were of sufficient length to access groundwater present in Glory Hole Cave.

Thakur et al. (2013) characterized paleoclimatic variations during the mid-Pleistocene transition (i.e. 1.8 Mya to 1.2 kya). Application of the SCWT to both solar radiation and delta-oxygen-18 data improved estimation of the relative contributions of three variables of the Earth's orbit to paleoclimate variations: precession (axial wobble), obliquity (axial tilt) and eccentricity (orbital divergence from a perfect circle). Herrera et al. (2014) characterized seismic trace data from a sedimentary basin in Canada containing Cretaceous age meandering channels. In comparison to results obtained from the CWT, the use of synchrosqueezing improved identification of multiple reflectors at arrival times ranging up to one second. Bian et al. (2018) characterized ocean wave turbulence and Reynolds stress. The SCWT was found to out-perform three other methods (i.e., coherence, co-spectra, and ensemble empirical mode decomposition), due in part to the ability to calculate time series of the instantaneous Reynolds stress. In the present study, the SCWT was implemented using the Synchrosqueezing Toolbox for MATLAB (Brevdo and Wu, 2011).

2.4. Empirical mode decomposition with Huang-Hilbert transform

Huang et al. (1998) derived an empirical method of decomposing time series data into a linear sum of cubic spline basis functions, known as intrinsic mode functions (IMFs). IMFs are calculated through an iterative procedure known as sifting, in which they are successively subtracted from the dataset until a zero-valued residual is obtained. The mean frequency of each IMF decreases during each iteration, which is characterized using a power law relation (Massei and Fournier, 2012). The Hilbert transform can be applied to each mode in order to calculate instantaneous frequencies, amplitudes and phases. The Hilbert transform, $y(t)$, of a given function $x(t)$ is defined as (Huang et al., 1998):

$$y(t) = \frac{1}{\pi} PV \int_{-\infty}^{+\infty} \frac{x(\tau)}{t-\tau} d\tau \quad \text{Equation 5}$$

where PV is the Cauchy principle value, which is used to avoid solutions of the integral that are equal to ± infinity, by converting them to a real value such as zero. The sum of the original time series and the Hilbert-transformed function is a complex-valued analytic function; i.e.:

$$z(t) = x(t) + i\, y(t) \quad \text{Equation 6}$$

Following Euler's identity, this relation can also be expressed in the form:

$$z(t) = \alpha(t)\, e^{i\theta(t)} \quad \text{Equation 7}$$

which contains parameters that describe the instantaneous amplitude (α) and instantaneous phase (θ) at time *t*. These are distinct from the non-instantaneous amplitude and phase parameters used in traditional Fourier analyses that are calculated over the full length of a given time series. Conveniently, instantaneous amplitude and phase values can be calculated as functions of $x(t)$ and $y(t)$; i.e.:

$$\alpha(t) = \sqrt{x(t)^2 + y(t)^2} \quad \text{Equation 8}$$

$$\theta(t) = arctan\left[\frac{y(t)}{x(t)}\right] \quad \text{Equation 9}$$

This combination of methods is known as the empirical mode decomposition-Hilbert Huang transform (EMD-HHT, or often simply referred to as EMD). Applications of the EMD-HHT in geophysical, atmospheric and climate, and oceanographic studies were reviewed by Huang and Zu (2008). Applications of the EMD-HHT in hydrology include Huang et al. (2009a), Rudi et al. (2010), and Massei and Fournier (2012). Huang et al. (2009) decomposed daily flow data recorded over more than 20 years in two rivers in northern France of contrasting sizes: the Seine River (large) and the Wimereaux River (small). Correlations were identified between low frequency (i.e. large period) modes in both rivers. It was hypothesized that both rivers were influenced by the maritime climate of northern France. Power relations between successive modes were used to assess flow intermittency. A power law relationship identified from the Seine River dataset indicated that dominant flow drivers were associated with processes occurring over 5–60 days, which correspond to synoptic and inter-seasonal scales. A similar

relationship was not observed in the Wimereaux River dataset, which indicated greater intermittency and greater sensitivity to local scale precipitation events.

Rudi et al. (2010) characterized runoff in the Upper Ruhr, Kall and Erkenskur rivers, all of which are located in the Ruhr River catchment of western Germany. Due to the proximity of the gauging stations used in this study (all of which were located within a $10km^2$ area), differences between estimated IMFs were limited. Results produced using the EMD-HHT were compared to those based on the STFT and CWT. The EMD-HHT was found to be superior to the STFT in two respects. First, EMD-HHT results were more localized, whereas STFT featured considerable "smearing" of energies due to spectral leakage. Second, while EMD-HHT results provided information at periods ranging from one to 256 days, STFT results did not contain information for periods less than 16 days. Massei and Fournier (2012) compared daily flow in the Seine River, France to the North Atlantic Oscillation. EMD-HHT results identified consistent timescales of variability; specifically, at inter-annual scales. The EMD-HHT method was capable of accounting for non-stationary processes in Seine River flow gauge data. In particular, for the first three estimated IMFs (i.e. representing the highest frequency basis functions), mean instantaneous amplitude values increased consistently after 1985. In the present study, the EMD-HHT was implemented using the PyEMD package for Python (Laszuk, 2020).

2.5. Complete ensemble empirical mode decomposition with adaptive noise

Since publication of the EMD-HHT approach, various improvements have been developed in order to increase the spectral separation between IMFs and to reduce the number of iterations required during the sifting procedure. Wu and Zhang (2009) derived the ensemble EMD method by including a Gaussian noise term when using ensemble averaging to estimate IMFs. The complete ensemble empirical mode decomposition with adaptive noise (CEEMDAN) method derived by Torres et al. (2011) enabled the sharing of noise parameter data between ensemble members.

Applications of the CEEMDAN method in hydrology include Antico et al. (2014), Adarsh and Reddy (2016), Reddy and Adarsh (2016), and Liu et al. (2018). Antico et al. (2014) used the CEEMDAN method to decompose and analyze the monthly mean discharge of the Parana River, South America. The authors identified dominant flow components at two distinct timescales: (1) annual and intra-annual oscillations that reflected seasonal precipitation; and (2)

inter-annual to inter-decadal variability. The latter was linked to three large scale climatic patterns: the El Nino Southern Oscillation, the North Atlantic Oscillation, and the Interdecadal Pacific Oscillation. In addition, non-stationary increases in river discharge fluxes were identified, which were attributed to anthropogenic climatic and land use changes. The CEEMDAN method was found to be superior to ensemble EMD for achieving frequency separation between intrinsic mode functions.

Reddy and Adarsh (2016) used the CEEMDAN approach to characterize monthly precipitation data from four meteorological subdivisions in India (i.e. Assam and Meghalaya, Kerala, Orissa, and Telangana) recorded over 142 years (i.e. 1871–2013). The CEEMDAN method was also used to characterize four large-scale climatic indices (i.e., the Atlantic Multidecadal Oscillation [AMO], the El Nino Southern Oscillation [ENSO], the Equatorial Indian Ocean Oscillation, and the Quasi-Biennial Oscillation [QBO]) and one solar index (i.e., the sunspot cycle). Analyses were undertaken on a seasonal basis: i.e., pre- and post-monsoon, monsoon, and winter. Qualitative comparisons indicated similarities to selected indices, which were quantified via cross-correlation analyses. In particular, the periodicity of individual IMFs was associated with specific indices. IMFs 1, 2 and 5 featured periodicities of 2–5, 5–7, >60 years respectively. These were associated with the QBO, ENSO and AMO indices respectively. IMFs 3 and 4 featured periodicities of 11 and 20–24 years, which were associated with the sunspot cycle and tidal forcing, respectively. Liu et al. (2018) used the CEEMDAN approach to characterize monthly precipitation in 12 sub-regions of Harbin, the capital of Heilongjiang Province in north-eastern China over a 49-year period (i.e. 1964–2013). The method was combined with the wavelet packet transform (Torresani, 1992) and multifractal detrended fluctuation analysis (Kantelhardt et al., 2002). Sub-regions featuring relatively low variability, and therefore greater predictability, were identified. Spatial variations in precipitation variability were compared to topographic, climatic, oceanographic and anthropogenic drivers. In the present study, the CEEMDAN approach was implemented using the PyEMD package for Python (Laszuk, 2020).

2.6. Nonlinear mode decomposition

The Nonlinear Mode Decomposition (NMD) method (Iatsenko 2015a; Iatsenko 2015b) combined aspects of existing Fourier, wavelet and EMD approaches. Either Fourier or wavelet

transforms can be used to generate a time-frequency representation of a given time series. The fundamental harmonic can be extracted from this representation and subsequently decomposed into a linear sum of frequency components. The parametric result, known as a nonlinear mode (NM) (and equivalent to an intrinsic mode function in EMD analysis), is then subtracted from the "raw" signal and the process is repeated until a pre-defined stopping criterion is met, resulting in the generation of a finite set of NMs. To date, the NMD approach has not been applied in hydrology. Published applications include for signal processing of underwater acoustic and electrocardiogram signals (Xin et al. 2016). In the present study, the NMD approach was implemented using the Nonlinear Mode Decomposition Toolbox for MATLAB (Iatsenko et al., 2015a).

2.7. Moving standard deviation

The moving standard deviation (MSD) method was first applied to temperature time series data to identify periods of streamflow by Blasch et al. (2004), and later modified by Assendelft and van Meerveld (2019). Here, the simplest version of this method was employed, in which the standard deviation of time series data, $\sigma(t)$, is calculated over a specified window size as:

$$\sigma(t) = \sqrt{\frac{1}{n-1}\sum_{i-t}^{n+t-1}[x_i - \bar{x}(t)]^2} \qquad \text{for } t = 1, \ldots, T \qquad \text{Equation 10}$$

where *n* is the number of measurements within the interval specified by the chosen window, $\bar{x}(t)$ is the average of the temperatures within the window, i is the sampling interval, t is the reference time, and T is the total number of measurements. As the window is moved successively forward in time across the time series, the moving standard deviation serves to magnify short-term (e.g. daily) variations in the thermal record, while minimizing larger-scale variability. For this application, a 0.5-day window size was chosen, with the reference time *t* centered within that window.

3. Methods

3.1. Synthetic example

An idealized synthetic temperature time series was used to demonstrate how the seven signal processing methods can be used to ascertain the presence or absence of stream flow. A flow signal with a 30 min sampling interval (i.e. 48 samples per day) was generated that comprised, in order of events: sub-daily (0.4 d), daily (1.0 d), and three multi-day flow events (3 × 4.0 d), with magnitudes of 1.0, 1.0, 3.0, 2.0, and 0.6 m^3/d (the units for flow in this example are arbitrary and only used to represent a differing magnitude). The first four signals are additive in nature, whereas the flow signal was used to dampen the sum of the other signals. A Wiener filter was used to dampen the signal amplitude in order to represent the presence of flow. The degree of dampening was related to the magnitude of flow, with larger flows indicated by stronger dampening.

Four components of real annual temperature signals that are typically observed at the surface of a streambed were added to the flow signal. These were:

1. A decadal-scale climate variation was represented using linear increasing trend (0.01 °C/d).
2. A seasonal variation due to tilt of the Earth was represented using a sinusoid with an amplitude of 30 °C, a period of 1 year, and an offset of 25 °C.
3. A daily variation due to rotation of the earth was represented using a sinusoid with an amplitude of 10 °C and a period of 1 d.
4. Signal noise representing local sub-daily variations in temperature (e.g. due to shading or wind) was represented using a continuous uniform distribution. For the low noise case, bounds of [-0.5, +0.5] °C were specified. For a high noise case, bounds of [-4, +4] °C. The range of the latter case (i.e. 8 °C) was chosen to ensure that the amplitude of fluctuations due to noise were of the same order of magnitude as "true" daily signals.

For each of the TF transform methods tested, it is possible to take a physically meaningful portion of one of the outputs and identify a threshold value that delineates between times of flow and no-flow. This threshold (x) was identified by minimizing an objective function $f(x)$, which was defined as:

$$f(x) = 1 - [0.5\,FM(x) + 0.5\,NFM(x)] \qquad \text{Equation 11}$$

where $FM(x)$ and $NFM(x)$ represent the fractions of flow and no-flow periods that were correctly identified when using threshold value x. Because a binary classification of the condition of flow or no-flow is used with the threshold, the output of the matching of flow (FM) and no-flow (NFM) results in a step function of matching whereby changes to the threshold might result in no change in the accuracy of the flow matching. This type of objective function can pose problems for gradient-based optimization approaches that rely on a numerically derived gradient due to the gradient becoming zero at non-optimal threshold values. Therefore, a stochastic differential evolution optimization approach (Storn and Price, 1997) was used, which was implemented using the Scipy package for Python (Virtanen et al., 2020). In the transform approaches applied, characteristic signals (seasonal and diurnal) should appear. The magnitude of the transform at diurnal frequency should in theory contain information on the magnitude of flow events.

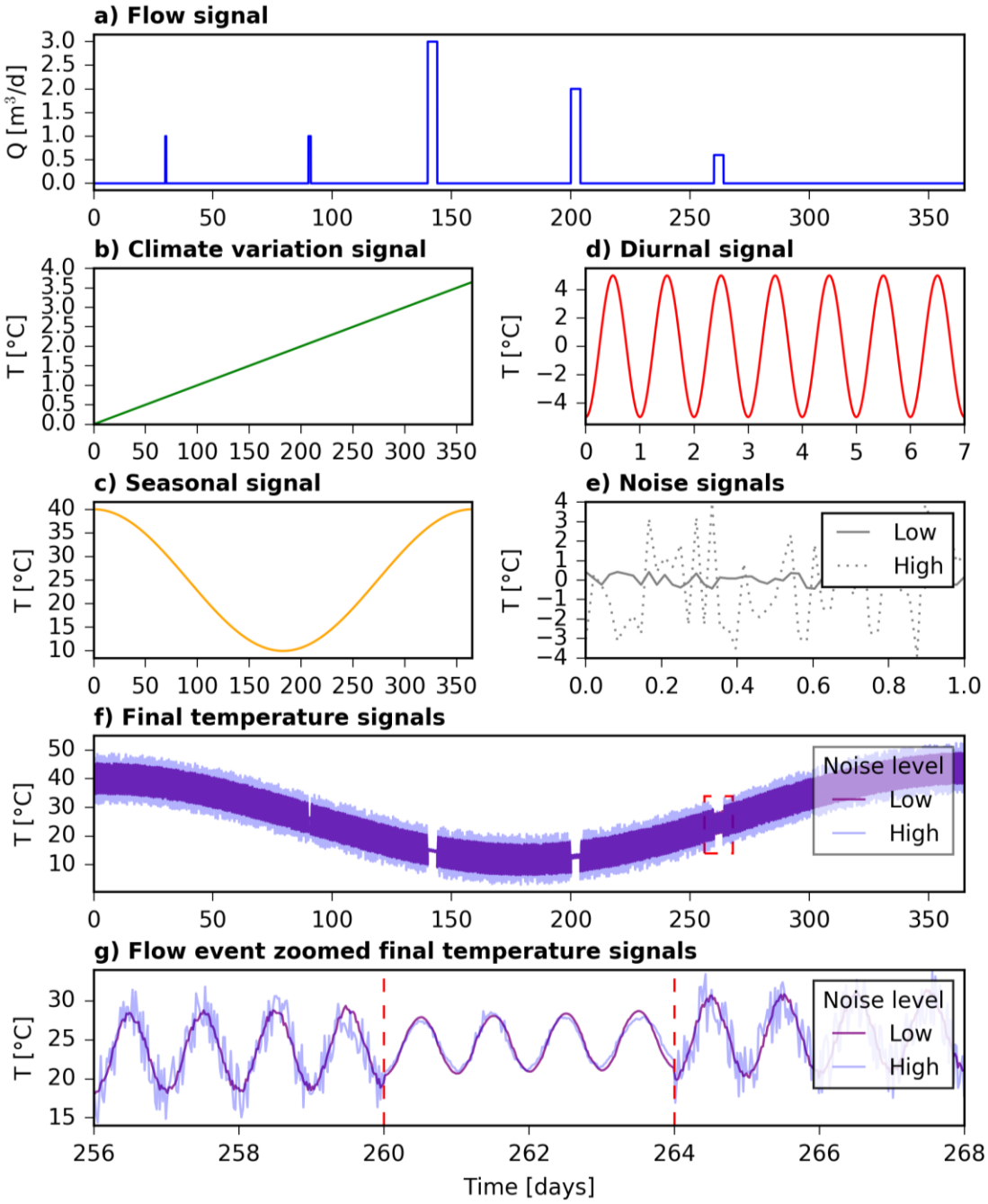

Figure 2. Synthetic temperature (T) time series for synthetic example. Input component signals included: (a) climatic variation; (b) annual seasonal variation; (c) diurnal fluctuation; (d) zero-mean white noise; and (e) flow period duration. (f) Resulting year-long temperature signal and (g) detailed view of days 256 to 268, showing attenuation of temperature fluctuations due to presence of stream water over sensor during ephemeral flow event.

3.2. Field example

In order to compare the efficacy of the seven methods when applied to a real-world dataset, stream flow and streambed temperature data were obtained from a gauging station located on Pedlar Creek near Kangarilla, South Australia (Station A5030503, Department of Environment and Water, Government of South Australia). Pedlar Creek drains an ephemeral and intermittent stream network located in a coastal, Mediterranean climate catchment in the Willunga Basin, located 25 km south of the city of Adelaide, South Australia. The creek typically flows from late June to mid-August (Figure 3), with annual streamflow in the range of 10^4–10^6 m^3 yr^{-1} (Shanafield et al., 2020) and standard deviation of 0.22. For this study, ~5 years of data from the period 2013 to 2018 were selected. The sampling interval used to analyze the data was 0.02 d (30 min).

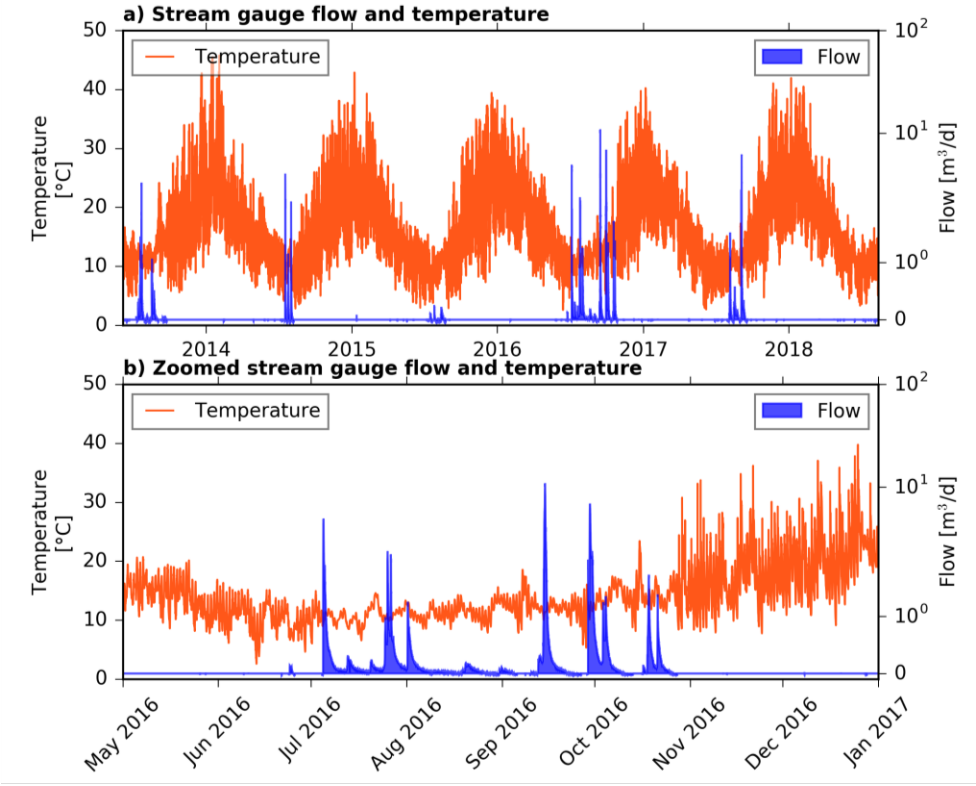

Figure 3. (a) Stream bed temperature and stream flow observations recorded on Pedlar Creek (Station A5030503) located near Kangarilla, South Australia, 2013–2018. (b) A subset of the same observations, shown for the period May–December 2016, which contains a series of flow events that demonstrate dampening of temperature signal amplitudes in the presence of flow.

4. Results

4.1. Synthetic example

Time-frequency transform analyses (Figure 4) focused on the 1 cycle per day (cpd) (i.e. diurnal) signal, as this is typically the dominant frequency (i.e. features the highest signal-to-noise ratio) observed in stream temperature observations (Stonestrom and Constantz, 2003). Each of the transforms showed a clear decrease in signal energy at the 1 cpd frequency during flow events. Reductions in energy at the 1 cpd frequency resulted in increases in energy at lower frequencies, which reduced the intensity of the amplitude spectra, which also signified flow events. Dampening of the temperature signal was observed, with the exception of the EMD spectra which indicated an increase in energy during flow events. Furthermore, larger magnitude flow events (and hence, greater attenuation of the temperature signal) enabled better discrimination of changes in flow for each of the methods. The onset of all synthetic flow events was evident in all transformed temperature signals to various degrees. In the high noise case, discrimination was less clear, particularly for shorter, low magnitude flow events.

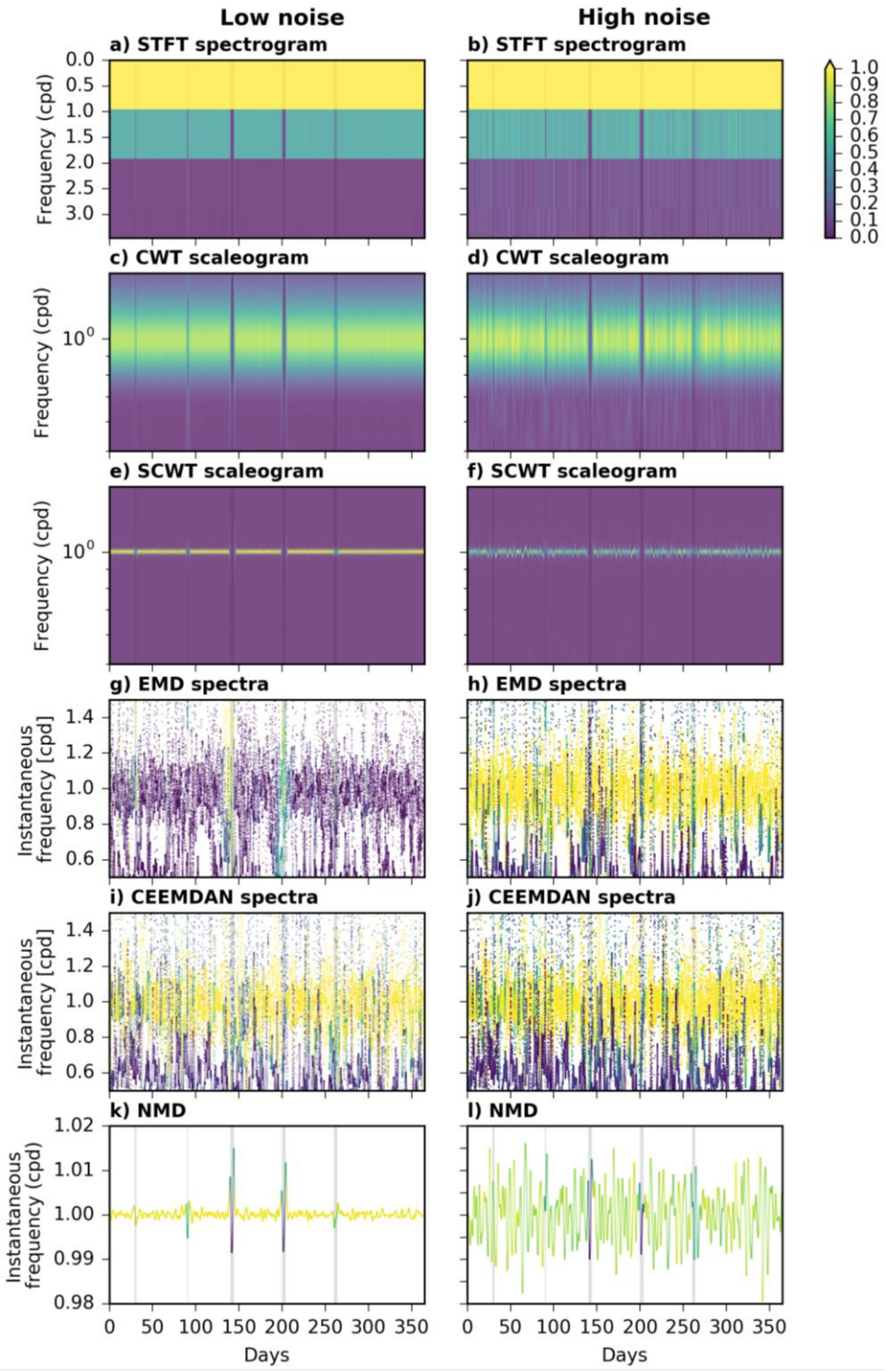

441

442 **Figure 4.** Amplitude and instantaneous amplitude results (with all values normalised to a [0,1]
443 range) derived from six time-frequency transform methods for low and high noise synthetic
444 temperature time series datasets. Flow events (light grey vertical bars) are presented to highlight
445 reductions in signal energy at these times. Note that results from the moving standard deviation
446 technique are not presented as this is not a time-frequency transform method.

447 To identify flow events, specific frequencies and modes were extracted (Figure 5). For
448 the STFT, CWT, and SCWT methods, time series at the 1 cpd frequency were extracted. For the
449 model decomposition methods, a single mode was selected for each method, based on visual
450 inspection. For the MSD method, only one output signal was generated, which was used to
451 identify flow events. Identification of flow and no-flow conditions using each method was based
452 on the differential evolution-obtained optimal threshold.

453 Most time-frequency approaches and the MSD method identified flow and no-flow
454 periods in the low noise case exactly, with flow matching of 100 % achieved. In contrast, the
455 EMD and CEEMDAN methods featured relatively lower flow matching values of 90.37 % and
456 92.70 % respectively. No-flow matching performance ranged from 95.18 % to 98.33 % across all
457 time-frequency transform methods, compared to a value of 99.07 % for the MSD method.
458 Misclassified flow and no flow periods were generally clustered around flow events, especially
459 for the time-frequency approaches. False negatives were observed both immediately before and
460 after flow events, in response to a sharp shifts in the amplitude or instantaneous amplitude of the
461 temperature signal. CEEMDAN method results also featured both false positives and negatives
462 scattered throughout the time series due to extremely noisy instantaneous amplitude values.

463 Results from the high noise case were more varied. While the STFT, SCWT, and MSD
464 methods achieved 100 % flow matching, flow delineation using EMD was compromised by the
465 noisy transformed signal (FM = 87.42 %). Large variability in instantaneous amplitude from
466 these methods resulted in flow delineation that was unrelated to known flow events, i.e. it was
467 not just a case of not identifying initiation or cessation of a flow event correctly but rather
468 misidentifying periods as flowing when no flow event occurred. The CWT, CEEMDAN and
469 NMD methods performed equally well, with flow matching of 96.89 % achieved in each case.
470 The proportion of no-flow periods successfully identified ranged from 98.29 % to 99.50 % for
471 each of the TF methods tested, with the exception of the SCWT method (77.29 %). As with the
472 low noise case, flow mismatches occurred directly prior to and after flow events, in response to
473 abrupt shifts in instantaneous amplitude values. Despite achieving the best overall matching of
474 flow and no-flow periods, the STFT and MSD approaches identified a considerable number of
475 false positives.
476

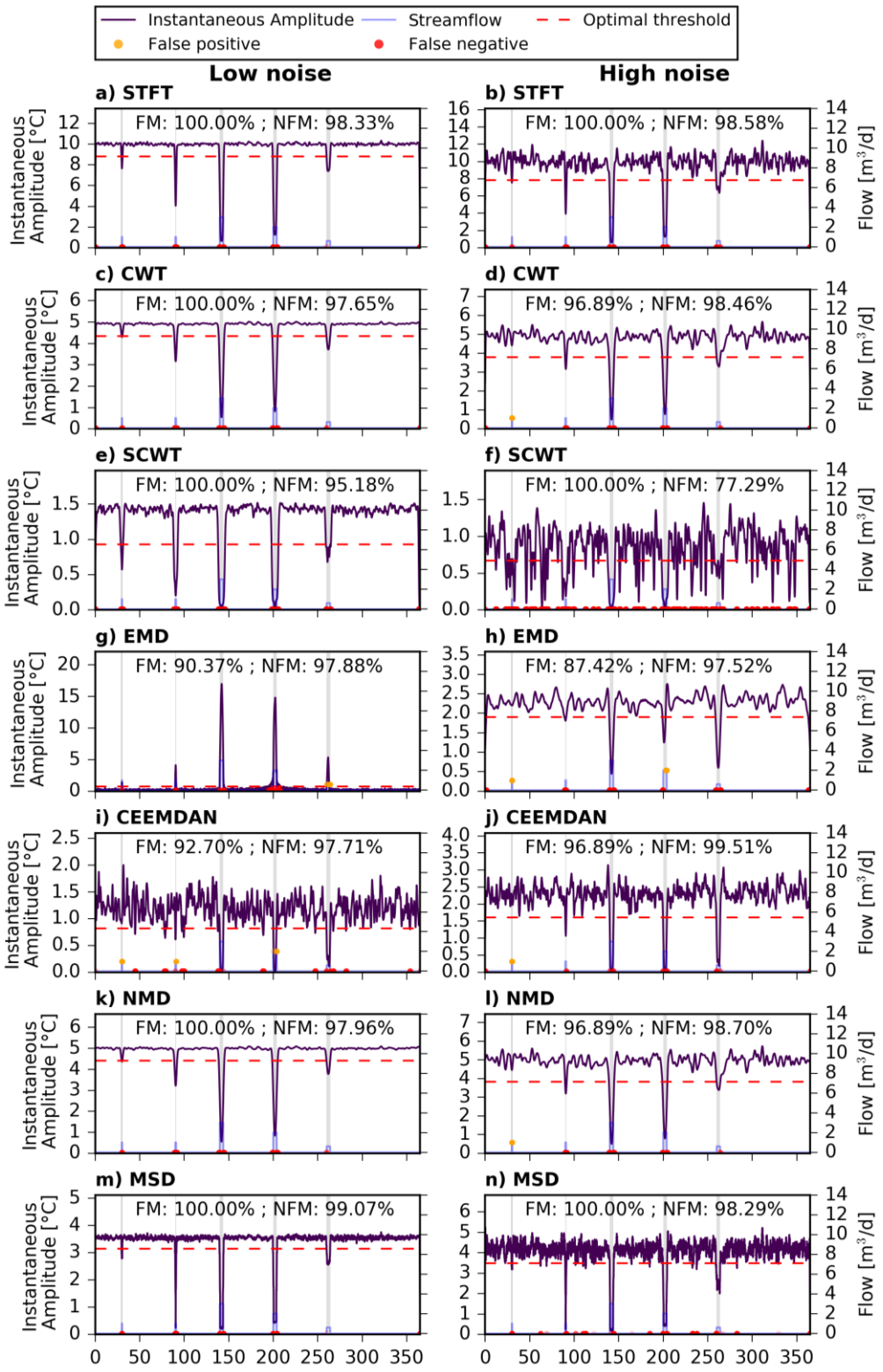

Figure 5. Optimal signal extracted from each of the seven methods tested (purple line) and corresponding optimized threshold frequency for delineating between flow and no-flow periods (red dashed line). Listed flow matching (FM) and no-flow matching (NFM) values summarise the proportion of flow and no-flow periods successfully identified, respectively.

4.2. Field Example

Application of time-frequency transform methods to the Kangarilla temperature signal dataset identified clear patterns for flow and no-flow periods around 1 cpd (Figure 6). Reductions in signal energy were proportional to the magnitudes of flow events. The CWT and NMD approaches performed relatively well, with flow matching greater than 99 % achieved (Figure 7). The EMD method performed relatively poorly, with flow matching of 88.01 % achieved. Flow matching for the remaining methods ranged from 90.44 % to 95.33 %. The matching of no-flow periods was markedly lower across all methods. No-flow matching ranged from 84.31 % to 89.44 %, with the exception of the SCWT method (63.66 %). The apparent noise present in the transformed temperature signal derived from the STFT, SCWT, EMD, CEEMDAN and MSD methods created a large number of incorrect classifications of flow. These occurred during no-flow periods that were not associated with any actual flow events, as well as at the end of both flow and no-flow periods. Overall, accurate classification of flow and no-flow periods for the field example dataset were achieved using the CWT and NMD methods. All intermittent flows were correctly predicted, but ephemeral flows less than one day were not.

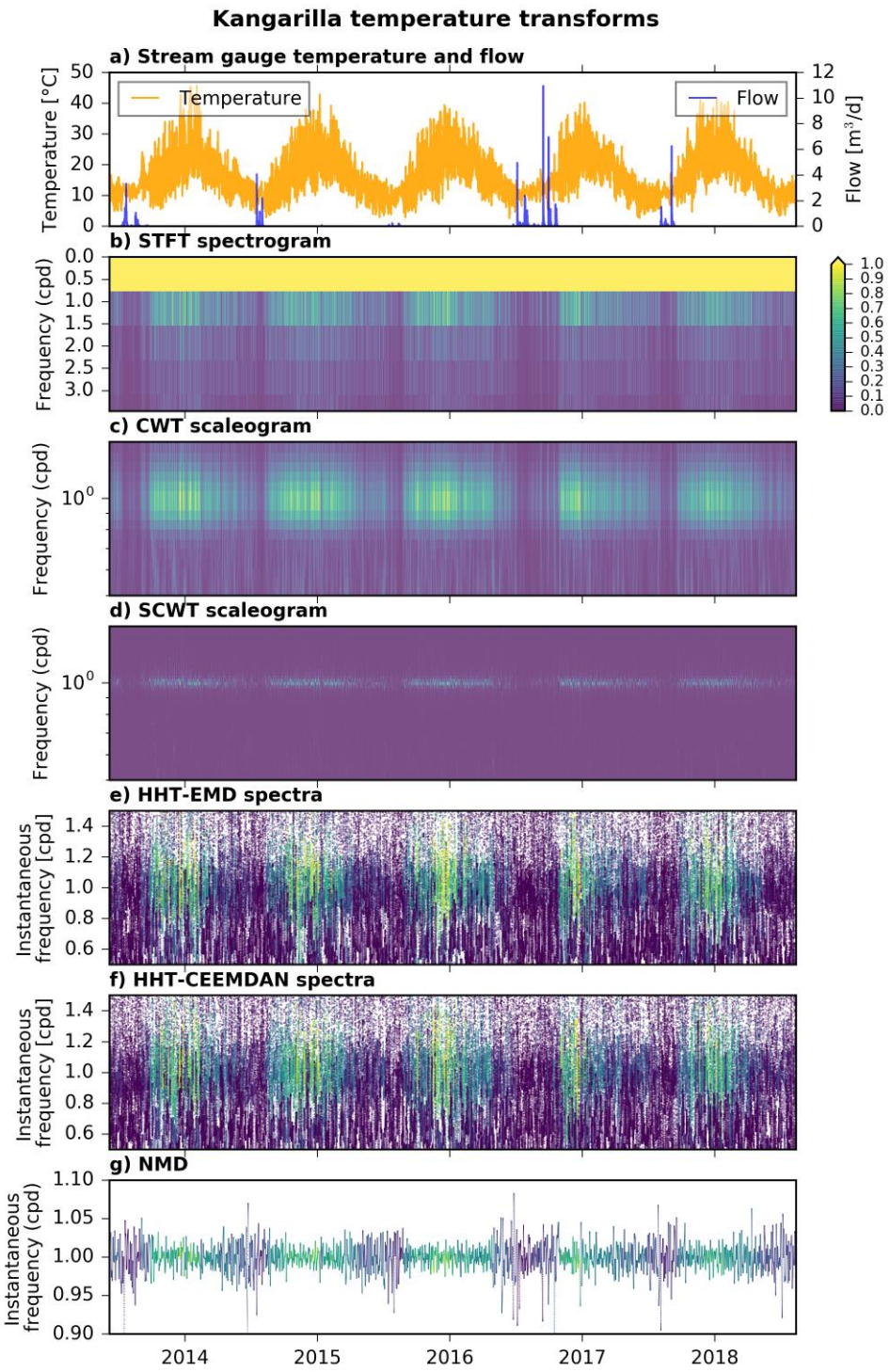

Figure 6. (a) Stream bed temperature and stream flow observations recorded on Pedlar Creek (Station A5030503) located near Kangarilla, South Australia, 2013–2018. Stream temperature and flow measurements from Pedlar Creek, South Australia. (b-g) Amplitude and instantaneous amplitude results (with all values normalised to a [0,1] range) derived using six time-frequency transform methods.

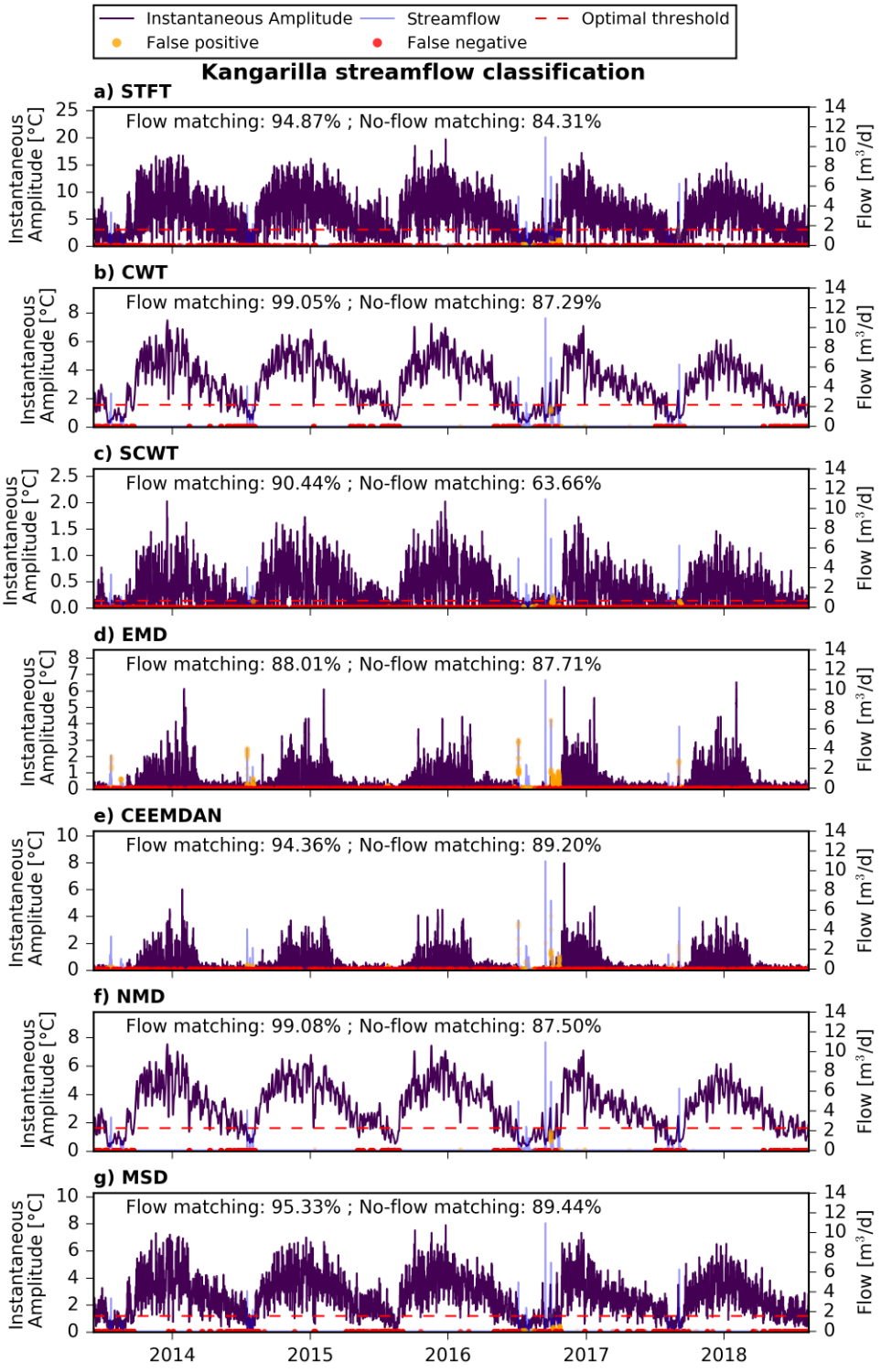

Figure 7. Identification of flow and no-flow periods from transformed Kangarilla streambed temperature time series dataset. Listed flow matching (FM) and no-flow matching (NFM) values summarize the proportion of flow and no-flow periods successfully identified, respectively.

5. Discussion

The aim of the present study was to identify time-frequency method(s) that are suitable for classifying stream flow states from streambed temperature time series data. The comparative merits of each method are now discussed. Take-home messages from the synthetic and real-world case studies are distilled. Suggestions for future research directions in terms of identifying flow presence using these methods are proposed.

5.1. Comparison of methods

Differences between the performance of the time-frequency methods tested in this study were found to be minimal, with all methods successfully identifying events greater than 1 day in duration. However, as in previous studies, evaluation of these methods was not achieved by simply comparing the success rate of successful flow or no-flow matching. Instead, it is important to consider several aspects of the method.

The main advantage of time-frequency methods over moving standard deviation approaches is the potential to develop a more objective, non-site-specific analysis that can be applied at multiple locations. For example, Assendelft and van Meerveld (2019) found that applications of simple moving standard deviation methods to stream temperature data did not adequately identify flow states during periodic flow events. The authors added several subjective criteria to their analysis in order to improve their results. In comparison, in this study we have simply applied a default approach across all methods. We expect that, as with the moving standard deviation approach, fine tuning of the methodology (e.g. experimentation with input parameters such as mother wavelet type or wave number, or improved means of determining threshold values) would further improve flow and no-flow matching capabilities.

The efficacy of time-frequency methods was found to be equal to or better than the moving standard deviation approach, without the need for subjective post-processing of results, and while offering the advantage of applicability at a catchment scale. Advantages of TF methods include their ease of use and in the minimal requirement for assumptions. For example, the STFT is widely used in hydrologic applications but requires the assumption that processes of interest are stationary within a specified window size. Processes such as the onset and cessation

of streamflow are by definition non-stationary. Identification of discrete changes in states using the STFT can be difficult and depends upon the length and sampling frequency of an observed dataset.

In comparison, the CWT method avoids the need for compromises between sampling resolution and measurement duration. The CWT is a more parsimonious approach than other time-frequency methods, is able to accommodate missing values in input datasets, is relatively intuitive in its theory, and mis-identified fewer flow events in comparison to STFT and MSD methods. The CWT can easily be implemented in MATLAB, R, Python, or other high-level languages, and periods of flow are relatively easy to identify from visual inspection of CWT outputs (e.g. Figures 3 and 5). Smearing effects may be present in CWT results but can be reduced through weighting of the CWT phase shift parameter. The synchrosqueezed CWT (which is currently only available in MATLAB), performed on par with CWT, but was not found to provide any additional benefits to the CWT for the test cases presented.

Mode decomposition methods were found to be less well-suited to the case studies presented, with generally slightly lower flow and no-flow matching accuracies and longer computing times. When identifying streamflow, the 1 cpd (i.e. diurnal) frequency was known to be the focus *a priori,* whereas mode methods contain energy from multiple frequencies. There is no physical basis for selecting a given mode. Mode decomposition methods are unable to accommodate missing values in input datasets, and streambed temperature measurements typically contain numerous data gaps, due to field conditions and equipment issues. However, the EMD method did identify long period seasonal variations, so this method may be useful for detrending of data prior to analysis. The CEEMDAN approach did not provide any advantage over the traditional EMD approach, and although the NMD method did perform well for flow matching, it was the most computationally cumbersome method tested.

5.2. Insights from applications to a real-world temperature dataset

The synthetic examples identified two metrics that best identified the onset and duration of flow events. The first was the ratio of temperature variance to noise strength. The second was the strength of a “flow” signal whereby it is necessary to see enough dampening of the temperature time series in order to clearly classify when it is flowing and not flowing correctly. Field data invariably includes a strong “noise” signal, due to climatic forcing, variation in

shading, micro-climates within the stream channel, and a variety of other factors. Moreover, the application of TF methods to real-world temperature time series data can be confounded by various aspects that were not represented in the synthetic examples provided in the present study.

These real-world factors were apparent in our field example, highlighting subtle differences between the results of the various methods. The Kangarilla field example showed that cessation of flow is typically more difficult to predict than the onset of flow. This may be due to pooling, which occurs in many intermittent rivers. Greater variation in amplitude values over time may be observed in real-world datasets, a trend which was clear with larger variance in temperature in the summer then in the winter. Also, temperature drops often accompany rainfall events. These lower the streambed temperature and thereby affect interpretation, allowing mis-classification of flow just prior to the onset of flow in the stream.

The interpretation of streamflow from streambed temperature time series data assumes the existence of a discernible diurnal temperature variation. Previous studies demonstrated that daily temperature variation in surface in shallow streams can be quite low, especially during spring and autumn (Anibas et al., 2009; Shanafield et al., 2017). This will preclude the application of such methods in some environments, such as low altitude, humid areas.

5.3. Future research directions

Applications of non-traditional time series analysis methods (i.e. other than Fourier and wavelet methods) in hydrology are currently limited. Published applications are generally restricted to direct observations of precipitation rates and discharge fluxes. Comparisons to exogenous datasets typically involved large-scale drivers such as climate indices. In comparison, in the present study, a range of traditional and non-traditional time series analysis methods were used to decompose a proxy measured variable (streambed surface temperature) in order to estimate a primary variable (stream flow), for physical processes occurring at sub-metre and sub-daily to daily to scales. The primary variable, stream flow, was also measured and provided the metric for method comparisons. This work provides a first step towards developing a method that can be automated to estimate streamflow state in non-perennial stream catchments without the need for either elaborate, expensive sensors or bespoke analysis routines.

Further research can greatly improve the methods presented in this study, including the following:

1. Rather than simply estimating flow state (as was the subject of this study), stream stage height could be estimated from the magnitude of signal dampening during flow events. This approach may be most appropriate for intermittent streams, for which the onset and duration of flow can be relatively well-known. We hypothesize that the ratio of air temperature variance to dampened streambed temperature variance could be used to distinguish between the two, as this ratio is dependent on the exposure of the sensor as well as the depth of flow.
2. In the present study, the 1 cpd (diurnal) frequency was known *a priori* to be the key frequency of interest. Additional investigations are required to determine whether other frequencies yield useful information for understanding stream functioning or flow states.
3. A temperature sampling frequency of 30 minutes was used in the present study. Future investigations should consider the impact of sampling frequency on ability to predict both start, continuation and end of flow events of varying timing and magnitude.
4. In the current application, the identification of flow state was limited to the daily scale, which is disadvantageous when compared to previous results of the moving standard deviation method. However, wavelet parameterisation may allow the identification of sub-daily (i.e. < 1 cpd) frequencies. For example, the frequency of the mother wavelet used in the CWT method is a function of the wave number specified, which in turn affects the amplitude of the output signal. The use of wave numbers lower than five should be investigated for their usefulness in identifying sub-daily flow events. Similarly, nested wavelet transforms, as used in the CEEMDAN approach, may assist the identification of transitions between flow states. However, the CEEMDAN method will remain subject to compromises between output resolution and smoothing.
5. As with the moving standard deviation method, the specification of a subjective, non-physical (and often site-specific) threshold value to delineate between flow and no-flow periods is unavoidable with time-frequency analysis techniques. Additional research is required to determine: whether a single threshold can be used to determine flow state for multiple sensors within a catchment; how the selection of the threshold can be numerically

625 optimized; or whether the threshold varies as a function of time (e.g. seasonally due to
626 variation in the amplitude of daily temperature oscillations).

627 ## 6. Conclusions

628 This work builds on several attempts to interpret stream flow states from streambed
629 temperature time series data. Most previous research compared the amplitudes of air and surface
630 water temperatures. Although such approaches have achieved limited success, it has been
631 proposed that air and surface temperature data alone are not sufficient for deducing the presence
632 of stream flows. Here, we examined the efficacy of non-stationary methods of temperature time
633 series analysis. While all methods were able to identify flow events at a daily scale, the CWT
634 method was identified as the most efficacious and most parsimonious. Benefits included the
635 ability to handle discontinuous datasets, ease of implementation and analysis, high performance,
636 and objectivity. Nevertheless, the implementation of CWT approaches presents ample
637 opportunities for improvement. In particular, more objective means of selecting flow/no-flow
638 threshold values are possible; for example, using automated optimization. Further
639 experimentation with algorithm inputs (such as wavelet wave number and convolution of output
640 frequencies) is likely to improve interpretation capabilities and extend the applicability of this
641 method across spatial (e.g. automation at a catchment scale) and temporal domains (e.g.
642 identification of sub-daily events).

643 ## Acknowledgments, Samples, and Data

644 The authors acknowledge the NCGRT NCRIS Super Science project for data for the
645 Kangarilla field site. NCRIS data is publicly available at http://groundwater.anu.edu.au/. We
646 thank Karina Gutiérrez-Jurado for processing the data. No other data was used for this study.
647 This research did not receive any specific grant from funding agencies in the public, commercial,
648 or not-for-profit sectors.

649 ## References

650 Abdollahi, S., Raeisi, J., Khalilianpour, M., Ahmadi, F., and Kisi, O. (2017). Daily mean
651 streamflow prediction in perennial and non-perennial rivers using four data driven
652 techniques. Water Resource Management, 31, 4855–4874. https://doi.org/10.1007/s11269-
653 017-1782-7

654 Adams, E. A., Monroe, S. A., Springer, A. E., Blasch, K. W., and Bills, D. J. (2006). Electrical
655 resistance sensors record spring flow timing, Grand Canyon, Arizona. *Ground Water*, *44*(5),
656 630–641.

657 Adarsh, S. and Reddy, M. J. (2016). Multiscale characterization of streamflow and suspended
658 sediment concentration data using Hilbert–Huang transform and time dependent intrinsic
659 correlation analysis. Modeling Earth Systems and Environment 2(4), 1-17.

660 Andreo, B., Jiménez, P., Durán, J. J., Carrasco, F., Vadillo, I., and Mangin, A. (2006). Climatic
661 and hydrological variations during the last 117–166 years in the south of the Iberian
662 Peninsula, from spectral and correlation analyses and continuous wavelet analyses.
663 Journal of Hydrology, 324(1-4), 24-39.

664 Anibas, C., Fleckenstein, J. H., Volze, N., Buis, K., Verhoeven, R., Meire, P., and Batelaan, O.
665 (2009). Transient or steady-state? Using vertical temperature profiles to quantify
666 groundwater–surface water exchange. Hydrological Processes, 23(15), 2165-2177.

667 Antico, A., Schlotthauer, G., and Torres, M. E. (2014). Analysis of hydroclimatic variability and
668 trends using a novel empirical mode decomposition: application to the Paraná River
669 Basin. Journal of Geophysical Research: Atmospheres, 119(3), 1218-1233.

670 Assendelft, R., and van Meerveld, H. J. (2019). A low-cost, multi-sensor system to monitor
671 temporary stream dynamics in mountainous headwater catchments. Sensors, 19(21), 4645.
672 https://doi.org/10.3390/s19214645

673 Bian, C., Liu, Z., Huang, Y., Zhao, L., and Jiang, W. (2018). On estimating turbulent Reynolds
674 stress in wavy aquatic environment. Journal of Geophysical Research: Oceans 123(4),
675 3060-3071.

676 Blasch, K. W., Ferre, T. P. A., Christensen, A. H., and Hoffmann, J. P. (2002). New field method
677 to determine streamflow timing using electrical resistance sensors. Vadose Zone Journal,
678 1(2), 289–299. https://doi.org/10.2113/1.2.289

679 Blasch, K. W., Ferré, T., and Hoffmann, J. P. (2004). A statistical technique for interpreting
680 streamflow timing using streambed sediment thermographs. Vadose Zone Journal 3(3),
681 936-946.

682 Blasch, K. W., Constantz, J., and Stonestrom, D. A. (2007). Thermal methods for investigating
683 groundwater recharge, U.S. Geological Survey Professional Paper 1703, Appendix 1,
684 351-373.

685 Brevdo, E. and Wu, H.-T. (2011) The Synchrosqueezing Toolbox,
686 https://web.math.princeton.edu/~ebrevdo/synsq/.

687 Chapin, T. P., Todd, A. S., and Zeigler, M. P. (2014). Robust, low-cost data loggers for stream
688 temperature, flow intermittency, and relative conductivity monitoring. Water Resources
689 Research, 50(8), 6542–6548. https://doi.org/10.1002/2013WR015158

690 Coleborn, K., Rau, G. C., Cuthbert, M. O., Baker, A., and Navarre, O. (2016). Solar-forced
691 diurnal regulation of cave drip rates via phreatophyte evapotranspiration. Hydrology and
692 Earth System Sciences, 20(11), 4439-4455.

693 Constantz, J., and Thomas, C. L. (1996). The use of streambed temperature profiles to estimate
694 the depth, duration, and rate of percolation beneath arroyos. Water Resources Research,
695 32(12), 3597-3602.

696 Constantz, J., and Thomas, C. L. (1997). Stream bed temperature profiles as indicators of
697 percolation characteristics beneath arroyos in the middle Rio Grande Basin, USA.
698 Hydrological Processes, 11(12), 1621-1634.

699 Constantz, J., Stonestorm, D., Stewart, A. E., Niswonger, R., and Smith, T. R. (2001). Analysis
700 of streambed temperatures in ephemeral channels to determine streamflow frequency and
701 duration. Water Resources Research, 37(2), 317-328.

702 Constantz, J., Stewart, A. E., Niswonger, R., and Sarma, L. (2002). Analysis of temperature
703 profiles for investigating stream losses beneath ephemeral channels. Water Resources
704 Research, 38(12), 52-1—52-13.

705 Costigan, K. H., Jaeger, K. L., Goss, C. W., Fritz, K. M., and Goebel, P. C. (2016).
706 Understanding controls on flow permanence in intermittent rivers to aid ecological research:
707 Integrating meteorology, geology and land cover. Ecohydrology, 9(7), 1141-1153.
708 https://doi.org/10.1002/eco.1712

709 Dadu K.S. and Deka P.C. (2016). Applications of wavelet transform technique in hydrology—A
710 brief review. In: Sarma A., Singh V., Kartha S., Bhattacharjya R. (ed.s) Urban Hydrology,

711 Watershed Management and Socio-Economic Aspects. Water Science and Technology
712 Library, vol. 73. Springer, Switzerland.

713 Datry, T., Larned, S. T., and Tockner, K. (2014). Intermittent Rivers: A Challenge for
714 Freshwater Ecology. BioScience, 64(3), 229–235. https://doi.org/10.1093/biosci/bit027

715 Datry, T., Fritz, K., and Leigh, C. (2016). Challenges, developments and perspectives in
716 intermittent river ecology. Freshwater Biology, 61(8), 1171–1180.
717 https://doi.org/10.1111/fwb.12789

718 Daubechies, I. (1990). The wavelet transform, time-frequency localization and signal analysis.
719 IEEE Transactions on Information Theory, 36(5), 961-1005.

720 Daubechies, I., Lu, J., and Wu, H. T. (2011). Synchrosqueezed wavelet transforms: An empirical
721 mode decomposition-like tool. Applied and Computational Harmonic Analysis 30(2):
722 243-261.

723 Eng, K., Wolock, D. M., and Dettinger, M. D. (2016). Sensitivity of Intermittent Streams to
724 Climate Variations in the USA. River Research and Applications, 32(5), 885–895.
725 https://doi.org/10.1002/rra.2939

726 Epting, S. M., Hosen, J. D., Alexander, L. C., Lang, M. W., Armstrong, A. W., and Palmer, M.
727 A. (2018). Landscape metrics as predictors of hydrologic connectivity between Coastal
728 Plain forested wetlands and streams. Hydrological Processes, 32(4), 516–532.
729 https://doi.org/10.1002/hyp.11433

730 Fritz, K., Johnson, B. R., and Walters, D. M. (2006). Field operations manual for assessing the
731 hydrologic permanence and ecological condition of headwater streams. EPA600/R-06/126,
732 U.S. Environmental Protection Agency, Office of Research and Development, Washington,
733 DC, USA, 152p. https://doi.org/10.13140/RG.2.1.4938.2245

734 De Girolamo, A. M., Lo Porto, A., Pappagallo, G., Tzoraki, O., and Gallart, F. (2015). The
735 hydrological status concept: Application at a temporary river (Candelaro, Italy). River
736 Research and Applications, 31(7), 892–903. https://doi.org/10.1002/rra.2786

737 Goulsbra, C. S., Lindsay, J. B., and Evans, M. G. (2009). A new approach to the application of
738 electrical resistance sensors to measuring the onset of ephemeral streamflow in wetland
739 environments. Water Resources Research, 45(9), W09501.

740 Grado, L. L., Johnson, M. D., and Netoff, T. I. (2017). The sliding windowed infinite Fourier
741 transform. IEEE Signal Processing Magazine 34(5): 183-188.)

742 Grossmann, A., and Morlet, J. (1984). Decomposition of Hardy functions into square integrable
743 wavelets of constant shape. SIAM Journal on Mathematical Analysis, 15(4): 723-736.

744 Gungle, B. W. (2005). Timing and duration of flow in ephemeral streams of the Sierra Vista
745 subwatershed of the Upper San Pedro Basin, Cochise County, Southeastern Arizona.
746 Scientific Investigations Report 2005-5190, U.S. Geological Survey, Reston, Virginia,
747 USA, 47p.

748 Herrera, R. H., Han, J., and van der Baan, M. (2014). Applications of the synchrosqueezing
749 transform in seismic time-frequency analysis. Geophysics, 79(3), V55-V64.

750 Huang, N. E., and Wu, Z. (2008). A review on Hilbert-Huang transform: Method and its
751 applications to geophysical studies. Reviews of Geophysics, 46(2), 1-23.

752 Huang, N. E., Shen, Z., Long, S. R., Wu, M. C., Shih, H. H., Zheng, Q., Yen, N.-C., Tung, C. C.,
753 and Liu, H. H. (1998). The empirical mode decomposition and the Hilbert spectrum for
754 nonlinear and non-stationary time series analysis. Proceedings of the Royal Society of
755 London. Series A: Mathematical, Physical and Engineering Sciences 454, 903-995.

756 Huang, Y., Schmitt, F. G., Lu, Z., and Liu, Y. (2009). Analysis of daily river flow fluctuations
757 using empirical mode decomposition and arbitrary order Hilbert spectral analysis. Journal
758 of Hydrology, 373(1-2), 103-111.

759 Huang, N. E., Wu, Z., Long, S. R., Arnold, K. C., Chen, X., and Blank, K. (2009). On
760 instantaneous frequency. Advances in Adaptive Data Analysis, 1(2), 177-229.

761 Iatsenko, D., McClintock, P. V., and Stefanovska, A. (2015a). Nonlinear mode decomposition: A
762 noise-robust, adaptive decomposition method. Physical Review E, 92(3), 032916-1–
763 032916-25.

764 Iatsenko, D. (2015b) Nonlinear Mode Decomposition: Theory and Applications. Springer,
765 Switzerland, 135p.

766 Jacobsen, E., and Lyons, R. (2003). The sliding DFT. IEEE Signal Processing Magazine, 20(2),
767 74-80.

768 Jaeger, K. L., and Olden, J. D. (2011). Electrical resistance sensor arrays as a means to quantify
769 longitudinal connectivity of rivers. River Research and Applications, 28(10), 1843-1852.

770 Jensen, C. K., McGuire, K. J., McLaughlin, D. L., and Scott, D. T. (2019). Quantifying
771 spatiotemporal variation in headwater stream length using flow intermittency sensors.
772 Environmental Monitoring and Assessment, 191(4). https://doi.org/10.1007/s10661-019-
773 7373-8

774 Jothiprakash, V. (2009). Rainfall-runoff models using adaptive neuro-fuzzy inference system
775 (ANFIS) for an intermittent river. International Journal of Artificial Intelligence, 3, 1-23.

776 Kantelhardt, J. W., Zschiegner, S. A., Koscielny-Bunde, E., Havlin, S., Bunde, A., and Stanley,
777 H. E. (2002). Multifractal detrended fluctuation analysis of non-stationary time series.
778 Physica A: Statistical Mechanics and its Applications, 316(1-4), 87-114.

779 Kunkel, M. L., and Pierce, J. L. (2010). Reconstructing snowmelt in Idaho's watershed using
780 historic streamflow records. Climatic Change, 98(1-2), 155-176.

781 Labat, D., Ababou, R., and Mangin, A. (2000a). Rainfall-runoff relations for karstic springs. Part
782 I: Convolution and spectral analyses. Journal of Hydrology, 238(3-4), 123-148.

783 Labat, D., Ababou, R., and Mangin, A. (2000b). Rainfall-runoff relations for karstic springs. Part
784 II: Continuous wavelet and discrete orthogonal multiresolution analyses. Journal of
785 Hydrology, 238(3-4), 149-178.

786 Labat, D. (2005). Recent advances in wavelet analyses: Part 1. A review of concepts. Journal of
787 Hydrology, 314(1-4), 275-288. https://doi.org/10.1016/j.jhydrol.2005.04.003

788 Labat, D., Ronchail, J., and Guyot, J. L. (2005). Recent advances in wavelet analyses: Part 2 -
789 Amazon, Parana, Orinoco and Congo discharges time scale variability. Journal of
790 Hydrology, 314(1-4), 289-311. https://doi.org/10.1016/j.jhydrol.2005.04.004

791 Laszuk, D. (2020). PyEMD Documentation, Release 0.2.9,
792 https://buildmedia.readthedocs.org/media/pdf/pyemd/latest/pyemd.pdf, accessed 21
793 August 2020.

794 Liu, D., Cheng, C., Fu, Q., Liu, C., Li, M., Faiz, M. A., Tianxiao, L., Khan, M. I., and Cui, S.
795 (2018). Multifractal detrended fluctuation analysis of regional precipitation sequences
796 based on the CEEMDAN-WPT. Pure and Applied Geophysics, 175(8), 3069-3084.

797 Maier, H. R., and Dandy, G. C. (2000). Neural networks for the prediction and forecasting of
798 water resources variables: A review of modelling issues and applications. Environmental
799 Modelling and Software, 15(1), 101-124. https://doi.org/10.1016/S1364-8152(99)00007-9

800 Massei, N., and Fournier, M. (2012). Assessing the expression of large-scale climatic
801 fluctuations in the hydrological variability of daily Seine river flow (France) between
802 1950 and 2008 using Hilbert-Huang Transform. Journal of Hydrology, 448, 119-128.

803 Morin, E., Grodek, T., Dahan, O., Benito, G., Kulls, C., Jacoby, Y., Van Langenhove, G., Seely,
804 M. and Enzel, Y. (2009). Flood routing and alluvial aquifer recharge along the ephemeral
805 arid Kuiseb River, Namibia. Journal of Hydrology, 368(1), 262-275.

806 Misiti, Y. Misiti, G. Oppenheim, and Poggi, J.-M. (1996) Wavelet Toolbox User's Guide, vol.
807 15. MathWorks Inc., Natick, MA, USA.

808 Murata, T., Fukami, K., and Fukagata, K. (2020). Nonlinear mode decomposition with
809 convolutional neural networks for fluid dynamics. Journal of Fluid Mechanics, 882(A-
810 13), 1-15.

811 Niu, J., and Sivakumar, B. (2013). Scale-dependent synthetic streamflow generation using a
812 continuous wavelet transform. Journal of Hydrology, 496, 71-78.

813 Percival, D. B. and Walden, A. T. (2006). Wavelet Methods for Time Series Analysis.
814 Cambridge University Press, Cambridge, U. K., 594p.

815 Peirce, S.E.and Lindsay, J.B. (2015). Characterizing ephemeral streams in a southern Ontario
816 watershed using electrical resistance sensors. Hydrological Processes, 29, 103-111.

817 Rao, A. R., and Hsu, E. C. (2008). Hilbert-Huang Transform Analysis of Hydrological and
818 Environmental Time Series. Water Science and Technology Library, vol. 60, Springer
819 Science and Business Media, 251p.

820 Rau, G. C., Halloran, L. J. S., Cuthbert, M. O., Andersen, M. S., Acworth, R. I., and Tellam, J.
821 H. (2017). Characterising the dynamics of surface water-groundwater interactions in

intermittent and ephemeral streams using streambed thermal signatures. Advances in Water Resources, 107, 354-369. https://doi.org/10.1016/j.advwatres.2017.07.005

Reddy, M. J., and Adarsh, S. (2016). Time–frequency characterization of sub-divisional scale seasonal rainfall in India using the Hilbert–Huang transform. Stochastic Environmental Research and Risk Assessment, 30(4), 1063-1085.

Rhif, M., Ben Abbes, A., Farah, I. R., Martínez, B., and Sang, Y. (2019). Wavelet transform application for/in non-stationary time series analysis: A review. Applied Sciences 9(1345): 1-22.

Richardson, L. F., and Eddy, W. F. (2019). Algorithm 991: The 2D Tree Sliding Window Discrete Fourier transform. ACM Transactions on Mathematical Software, 45(1), Article 12, 12 pages. https://doi.org/10.1145/3264426

Rodríguez-Burgueño, J. E., Shanafield, M., and Ramírez-Hernández, J. (2017). Comparison of infiltration rates in the dry riverbed of the Colorado River Delta during environmental flows. Ecological Engineering, 106. https://doi.org/10.1016/j.ecoleng.2017.02.014

Rudi, J., Pabel, R., Jager, G., Koch, R., Kunoth, A., and Bogena, H. (2010). Multiscale analysis of hydrologic time series data using the Hilbert–Huang transform. Vadose Zone Journal, 9(4), 925-942.

Sang, Y. F. (2013). A review on the applications of wavelet transform in hydrology time series analysis. Atmospheric Research, 122, 8-15.

Shanafield, M., Niswonger, R. G., Prudic, D. E., Pohll, G., Susfalk, R., and Panday, S. (2012). A method for estimating spatially-variable seepage and hydraulic conductivity in channels with very mild slopes. Hydrological Processes, 28(1), 51-61. https://doi.org/10.1002/hyp.9545

Shanafield, M., McCallum, J. L., Cook, P. G., and Noorduijn, S. (2017). Using basic metrics to analyze high-resolution temperature data in the subsurface. Hydrogeology Journal, 25(5), 1501-1508.

Stonestrom, D. A., and Constantz, J. (2003). Heat as a tool for studying the movement of ground water near streams, USGS Circular 1260. US Geological Survey, Denver, Colorado, USA.

Storn, R. and Price, K., (1997). Differential Evolution - a simple and efficient heuristic for global optimization over continuous spaces, Journal of Global Optimization, 11, 341-359.

Tary, J. B., Herrera, R. H., and van der Baan, M. (2018). Analysis of time-varying signals using continuous wavelet and synchrosqueezed transforms. Philosophical Transactions of the Royal Society A: Mathematical, Physical and Engineering Sciences, 376: 20170254. http://dx.doi.org/10.1098/rsta.2017.0254

Thakur, G., Brevdo, E., Fučkar, N. S., and Wu, H. T. (2013). The Synchrosqueezing algorithm for time-varying spectral analysis: Robustness properties and new paleoclimate applications. *Signal Processing*, *93*(5), 1079–1094. https://doi.org/10.1016/j.sigpro.2012.11.029

Tooth, S. (2000). Process, form and change in dryland rivers: A review of recent research. Earth-Science Reviews, 51(1), 67-107.

Torres, M. E., Colominas, M. A., Schlotthauer, G., and Flandrin, P. (2011). A complete ensemble empirical mode decomposition with adaptive noise. In: IEEE International Conference on Acoustics, Speech and Signal Processing (ICASSP), pp. 4144-4147.

Torresani, B. (1992). Time-frequency representations: Wavelet packets and optimal decomposition. Annales de l'Institut Henri Poincare C, Analyse Non Lineaire 56: 215-234.

Virtanen, P., Gommers, R., Oliphant, T. E., Haberland, M., Reddy, T., Cournapeau, D., Burovski, E., Peterson, P., Weckesser, W., Bright, J., van der Walt, S. J., Brett, M., Wilson, J., Millman, K. J., Mayorov, N., Nelson, A. R. J, Jones, E., Kern, R., Larson, E., Carey, C. J., Polat, I., Feng, Y., Moore, E. W., VanderPlas, J., Laxalde, D., Perktold, J., Cimrman, R., Henriksen, I., Quintero, E. A., Harris, C. R., Archibald, A. M., Ribeiro, A. H., Pedregosa, F., van Mulbregt, P., and SciPy 1.0 Contributors. (2020). SciPy 1.0: fundamental algorithms for scientific computing in Python. Nature Methods, 1-12.

van der Walt, S., Colbert, S. C., and Varoquaux, G. (2011). The NumPy array: a structure for efficient numerical computation. Computing in Science and Engineering, 13(2), 22-30.

Wu, Z. and Huang, N. E. (2009). Ensemble empirical mode de-composition: A noise-assisted data analysis method, Advances in Adaptive Data Analysis, 1(1), 1–41.

879 Xin, Z., Jie, S., Wenwei, A., Tiantian, Y., and Malekian, R. (2016). An improved time-frequency
880 representation based on nonlinear mode decomposition and adaptive optimal kernel.
881 Elektronika ir Elektrotechnika, 22(4), 52-57.